Molecular Catalysis 478 (2019) 110566

Contents lists available at ScienceDirect

Molecular Catalysis

journal homepage: www.elsevier.com/locate/mcat

Effect of titania support on Fischer-Tropsch synthesis using cobalt, iron, and ruthenium catalysts in silicon-microchannel microreactor

Richard Y. Abrokwah[a,d], Mahbubur M. Rahman[b], Vishwanath G. Deshmane[a,b], Debasish Kuila[a,c,d,*]

[a] Department of Chemistry, North Carolina A & T State University, Greensboro, NC 27411, USA
[b] Department of Chemical Engineering, North Carolina A & T State University, Greensboro, NC 27411, USA
[c] Department of Nanoengineering, Joint School of Nanoscience and Nanoengineering, North Carolina A & T State University, Greensboro, NC 27411, USA
[d] Energy and Environmental Systems, North Carolina A & T State University, Greensboro, NC 27411, USA

ARTICLE INFO

Keywords:
TiO_2-support
Si-microreactor
Metal support interaction
Fischer-Tropsch
Syngas conversion

ABSTRACT

Syngas conversion into hydrocarbons using Fischer Tropsch (F-T) Synthesis was carried out to investigate the effect of TiO_2 support on catalytic performance using 12% by weight of metal -12Co-TiO_2, 12Fe-TiO_2 and 12Ru-TiO_2 in silicon (Si) microchannel microreactor (50 μm wide x100 μm deep) at different reaction temperatures and 1 atm. A modified closed channel infiltration (mCCI) method was used for successful uniform coating of the sol-gel catalyst layer in the micro-channels of Si-microrecators. Temperature Program Reduction profiles with H_2 showed interaction of TiO_2 with each metal to be significantly different; TPR of Fe-TiO_2 and Co-TiO_2 indicated a significant strong metal (Co and Fe) support interaction (SMSI), while that of Ru-TiO_2 suggested a weaker metal-support interaction. The XRD studies of the catalysts suggest that unlike Fe- and Co-TiO_2, Ru-TiO_2 consists of mixed anatase and rutile phases of TiO_2. The absence of rutile phase in Co-TiO_2 and Fe-TiO_2 had a profound effect on F-T activity in the range of 150 °C to 300 °C for CO conversion and hydrocarbon selectivity at 1 atm and decreased the stability of these two catalysts. The overall stability and reactivity was in the order: 12%Ru-TiO_2 > > 12%Fe-TiO_2 > 12%Co-TiO_2. These results are distinctly different from our previous studies with silica sol-gel in microreactor where a reverse trend was observed.

Introduction

Since the invention of the FT process in Germany 1920 by Franz Fisher and Hanz Tropsch, the reactions have been carried out in traditional gigantic tubular fixed bed and slurry bubble-column reactors. Exxon Mobil, Sasol, Shell and ConoPhilips have been the trailblazers of technological advancements as well as catalyst development and formulations for gas to liquid (GTL) fuel synthesis. Dieter Leckel of Sasol [1] reported on the successes and milestones accomplished by these companies using high-temperature Fischer-Tropsch (HTFT) and the low-temperature Fischer-Tropsch (LTFT) processes. Dieter pointed out that these gigantic tubular reactors and distillates can produce over 140,000bpd of GTL products and 120,000boe/d of condensate, liquefied petroleum gas and ethane making them economically viable. Some of the critical shortfalls of these huge reactors are that they could be more than 60 m tall that takes long construction time and cannot be moved to offshores (on-site) or agricultural sites where syngas/feedstocks are generated (on demand) in smaller quantities. In addition, there are problems associated with the stability of the catalysts in these reactions. As an example, in 2007, Sasol reported the technical problems associated with generation of fine particles due to catalyst attrition in their slurry bubble column reactors during the Fischer Tropsch (F-T) reactions. [2]

Over the past decade, technological emergence of portable and mobile F-T microdevices and microreactors have gained attraction in numerous industrial applications. Velocys fuel Corporation has been at the forefront for the explication of advanced microchannel gas-to-liquids technologies for monetizing bio-syngas and waste gas reserves. Tonkovich and associates from Velocys [3] have outlined the techno-economic advantages of microchannel microreactors, also known as 'Lab-on-a-chip' devices (because they measure a few centimeters in length and volume). They asserted that these microdevices could significantly reduce the size of conventional chemical reactors without lowering the throughput. These high throughput-microreactors could supplement or partially replace the time-consuming, more expensive and manpower consuming conventional production technologies [3]

* Corresponding author at: Department of Chemistry, North Carolina A & T State University, Greensboro, NC 27411, USA.
E-mail address: dkuila@ncat.edu (D. Kuila).

https://doi.org/10.1016/j.mcat.2019.110566
Received 15 May 2019; Received in revised form 6 August 2019; Accepted 14 August 2019
Available online 22 August 2019
2468-8231/

The microchannels of the microdevices do not affect the chemistry of a reaction because the underlying chemistry is performed at the molecular level [4]. Furthermore, as it has been reported by Lerou and coworkers, the microchannel reactor design enhances the formation of greener products and greener reaction pathways to fuels [5].

Development of microreactor technology indeed provides a platform of miniature chemical plants. The reaction zones in a microreactor are the microchannels, through which the fluid flows [6]. Controlling the reaction parameters such as temperature, pressure, and flowrate are relatively easier in a microreactor since the small parallel flow paths in microreactors with high aspect ratios (channel height to width ratio) strongly reduce the pressure drops. Due to the decrease in the length of the reactor and extremely small dimensions of the microchannels, the surface-to-volume ratio of the microstructures is significantly higher compared to the conventional reactors. The large surface-to-volume ratio of microchannels inhibits gas-phase free-radical reactions, improves and maintains isothermal heat transfer for exothermic reactions. The flow properties and residence times can be controlled precisely in these small devices to attain an optimum yield and selectivity of a specific reaction [6]. In order to boost production, microreactors do not need scaling up; rather, several microreactors could be juxta positioned and operated safely.

The catalysts used for CO hydrogenation in Fischer-Tropsch (F-T) reactions are characteristically identified based on their ability to dissociate the C—O bond in the first step of the reaction mechanism and promote the C—C bond formation. It has been observed that group VIII metals show increased activity for C—C coupling reaction during hydrogenation of carbon monoxide; iron, cobalt, and ruthenium are the most used catalyst systems for F-T reactions. [7,8] Iron catalyst have been used commercially by Sasol Corporation in F-T synthesis for the past six decades [9]. It has several advantages over other catalysts such as affordability, preferred catalysts at high temperatures with increased water gas shift reaction, hence ideal for syngas feed with relatively low H_2/CO ratio. It also has high activity for the production of higher alkanes that can be used directly as gasoline and also for the production of olefinic compounds necessary as a chemical feedstock for various chemical reactions [10]. Iron oxide, iron carbide and its carbonitrides are the most commonly used F-T catalysts; the most active phase is the iron carbide. In general, the water-gas shift (WGS) reaction, mostly favored by iron catalysts, produces carbon dioxide with low selectivity towards hydrocarbons, making them inherently unstable, resulting in deactivation and loss of catalytic property. However, the activity of these catalysts is enhanced in the presence of copper and alkali metals [6].

In contrast to the iron catalyst, FTS reaction on cobalt catalyst is highly dynamic depending strongly on the partial pressure of reactants, temperature, and reactor residence time [11]. The active phase of cobalt catalyst is pure metallic cobalt, mostly used for low-temperature reactions with hydrogen-rich sources like natural gas-based syngas. Cobalt catalysts have less tendency to water gas shift (WGS) activity and result in the formation of very active and linear hydrocarbon with higher selectivity when used with noble metal promoters [6]. Furthermore, it has been reported that cobalt catalyst reduces the formation of carbides that are precursors to the formation of coke and hence increase the catalyst life [12]. These catalysts are expensive and used with metal oxide supports for better stability.

Compared to Fe, Co is known to be a very active and suitable catalyst for hydrogenation of carbon monoxide. It shows promising conversion with higher hydrocarbon selectivity during FTS reaction [11]. Ruthenium is also known to make higher alcohols as an alternative to higher alkanes. Therefore, a correct understanding of the process parameters like pressure, temperature and feed ratios is needed to optimize its use for FTS reaction [13]. Although ruthenium is a very good catalyst for fundamental studies of FTS, it is very expensive (around 50,000 times the price of iron).

In addition to metal catalysts described above, the catalyst support plays a very significant role in F-T synthesis. Many inorganic supports such as, zirconia, ceria, titania, carbon nanotubes, silica-zirconia, silica-alumina, tungsten-zirconia, sulfated zirconia [14,15], SiO_2 [16–18], Al_2O_3 [19,20], TiO_2 [21–23] and zeolites [24–26] for anchoring different catalysts have been studied extensively for years. Support largely influences the oxidation state of metal, particle size and the degree of reduction. For example, Co-oxide species in SiO_2 gets reduced easily to large Co-particles in H_2 atmosphere at relatively low temperature as the interaction between SiO_2 and cobalt is weak. In contrast, much higher temperature is required for reduction of Co-oxides in Al_2O_3 due to stronger interaction between Co and Al_2O_3. Small Co- metal particles tend to be formed on Al_2O_3. The interaction between metal and TiO_2 is in between SiO_2 and Al_2O_3.

For F-T reactions, conversion of CO and hydrocarbon product distribution has been shown to be a function of catalyst preparation and reaction conditions. For instance, Jothimurugesan and Gangwal observed CH_4 selectivity from 10% to 34% depending on the reaction parameters [27]. Duvenhage et al. [28] also showed that variability in CH_4 and longer chain hydrocarbon selectivity depended on the calcination and reduction temperature. Duvenhage and Coville further demonstrated that the method of catalyst preparation played a major role in hydrocarbon product distribution [29]. They inferred that catalyst prepared by impregnation using carbonyl precursors yielded very low amounts of CH_4 while those prepared by precipitation technique produced over 20% CH_4. In our previous F-T studies [30], we used Co, Fe and Ru in silica using Si-microchannel microreactor. We observed that the reaction temperature, the type of metal and the H_2/CO mole ratio were critical for maximum CO conversion and hydrocarbon fuel selectivity. For example, at 250 °C and H_2/CO mole ratio of 2:1 Ru/SiO_2 showed the highest FT reactivity and Fe/SiO_2 the least. However, Co/SiO_2 showed the highest ˜90% CO conversion. Furthermore, after continuous 72 h FT reaction, Co/SiO_2 catalyst showed the highest stability followed by Fe/SiO_2 while Ru/SiO_2 exhibited the least stability. One of the major objectives of this present study is to investigate the effect of TiO_2 support on metals such as Co, Fe and Ru since no previous studies using TiO_2 sol-gel coated in a microreactor has been reported. While TiO_2 is suitable for practical applications due to its low cost, safety and chemical stability; it has been reported that the strength of Co-TiO_2 interaction is in the middle of Co/SiO_2 and Co/Al_2O_3. Thus, we envisaged that the metal particles with higher reducibility can be obtained in our studies. Further, we hypothesized that the strong electronic and metal interaction properties of nanocrystalline TiO_2 support could enhance the selectivity and yield of synfuels in a microreactor and more specifically can be tuned by the effect of reaction temperature. More significantly, we wanted to compare these catalysts in TiO_2 to our previous F-T studies in silica support.

In this paper, we report successful coating of the michrochannels of a Si-microreactor with TiO_2 sol gel catalysts and show that C_1-C_4 hydrocarbons or synfuels are formed at 1 atm. Compared to our previous work with SiO_2 supported catalysts, we have ascertained that Co, Fe, & Ru behave quite differently on TiO_2 due to effects of different polymorphs of the TiO_2. Indeed, the morphology and crystal phase of TiO_2 have a profound effect on conversion, stability of the catalysts, and selectivity of the produced synfuels at 1 atm in the Si-microreactor. Both F-T activity and stability in TiO_2 are conspicuously different, i.e. Ru-TiO_2 > > Fe-TiO_2 > > Co-TiO_2 in contrast to our previous studies with silica support.

Materials and methods

The reagents procured and used for synthesis of the sol-gel catalysts. Titanium Isopropoxide, Ruthenium (111) Chloride, Iron (III) Nitrate Nonahydrate and Nitric acid were purchased from ACROS ORGANICS. Cobalt (II) Nitrate Hexahydrate was purchased from Sigma-Aldrich. Silicon wafers- single side polished, 100 mm diameter, and 500 µm thick wafers were procured from Louisiana (LA) Tech University for the

microfabrication of the microreactors. The F-T reactions were carried out by simulating synthesis gas involving the composition of H_2 and CO gases. Ultra- high pure H_2 from AIR LIQUIDE, Plumstead Ville, PA, USA, and 98% pure CO from Air gas were procured for the reaction. 5.0 grade (99.999%) He from Machine and Welding Supply Corporation. Greemsboro, NC was used, as a carrier of the reaction product gases. Ultra-high purity N_2 from Machine and Welding Supply Corporation was used as the reaction internal standard and for BET surface area analysis. For the reduction of the catalysts, 10/90 vol percentage of H_2/Ar was used from Machine and Welding Supply Corporation. To maintain an inert environment inside the furnace prior to reduction of the catalyst, it was purged using 5.0 grade N_2 gas.

Fabrication of silicon microreactors

The complete fabrication process is based on previous work performed at Louisiana Tech University [31]. The microreactors were fabricated by a lithographic process followed by Deep Reactive Ion Etching (DRIE). Prior to microfabrication of the microchannel silicon microreactors, the silicon wafers of 100 mm diameter and 500 µm thick were procured. The design of the microreactor is based on a split and recombination principle. The technology involves pyramidal divisions of inlets and outlets into numerous sublets for controlled diffusion of the gases (reactants and products) into and out of the straight channels. Two types of microchannel silicon microreactors were used in our studies. The initial dimensions of the wafers containing 116 straight channels and 1.3 cm long were either (a) 50 µm wide, 80 µm deep, or (b) 50 µm wide, 130 µm deep. The 50 µm wide by 100 µm deep microreactors were also fabricated at Louisiana (LA) Tech University using deep reactive ion etching (DRIE) technique.

Catalyst synthesis and coating of microreactor

Sol-gel chemistry was used for the preparation of the catalyst and coating of the microchannels. The precursor titanium isopropoxide (TTIP), ethanol, water, and acetylacetone are mixed in molar ratio 1:20:1:1, respectively [32]. For the preparation of titania sol-gel, nitric acid was used as a catalyst. Fig. 1 shows flow diagram for sol-gel synthesis. Acetyl acetone acts as a stabilizer that promotes a controlled hydrolysis-condensation process to ensure formation of a homogeneous polymeric gel instead of particulate sols [9]. TiO_2 sol was prepared by mixing TTIP: ethanol in a molar ratio of 1:10. Afterward, an acetylacetone stabilizer was added such that the molar ratio of acetylacetone to TTIP was unity. Then deionized water and ethanol were mixed and added slowly under continuous stirring to prevent precipitation of the sol. The final molar ratio of ethanol: TTIP in the sol then was 20, and the molar ratio of water: TTIP was one. Nitric acid (0.1 M) was then added dropwise to adjust the pH to 4.5; and the solution was stirred and heated at 40 °C for 24 h. The catalyst precursors were then added in proportions such that the metal loading was 12 wt% in the titania sol-gel. This mixture was then stirred (aged) at 40 °C for a week to bolster the catalyst surface area and proper encapsulation of the metal in the titania support [4]. Calcined microreactors and powder form of the catalysts were reduced under hydrogen/argon (10/90 vol ratio) atmosphere. The tubular furnace was first purged with nitrogen for 30 min in order to remove traces of air from the furnace. The flow rate of the hydrogen/argon mixture was set at 3.5 L/min at a heating ramp rate of 5 °C/min.

Catalyst Coating inside the microchannels of Si-microreactor

Catalyst loading in the microchannels is one of the most critical steps for effective use of this fabricated microdevice for chemical reactions. This step is done in several ways such as dip coating, drop coating, and sputter coating. These methods have been discussed in detail elsewhere [4]. An in-situ approach for loading the catalyst was used in this work to overcome the disadvantages of other methods mentioned in the literature. This method is called closed channel infiltration (CCI) method. For better sealing during catalyst coating, two compressible silicon gaskets were placed on either side of the microreactor. This ensures uniform coating as well as retention of the catalysts in the microchannels. The microreactor is placed between two aluminum heating blocks as shown in Fig. 2.

The inlet of the upper heating block is connected with C-FLEX tubing, after which the catalyst is suctioned into a syringe and pumped into the microreactor using a KD Scientific® syringe pump. In this method, the flowrate is kept very low and constant (i.e., around 0.08 ml/h), and the temperature was maintained at 30–40 °C

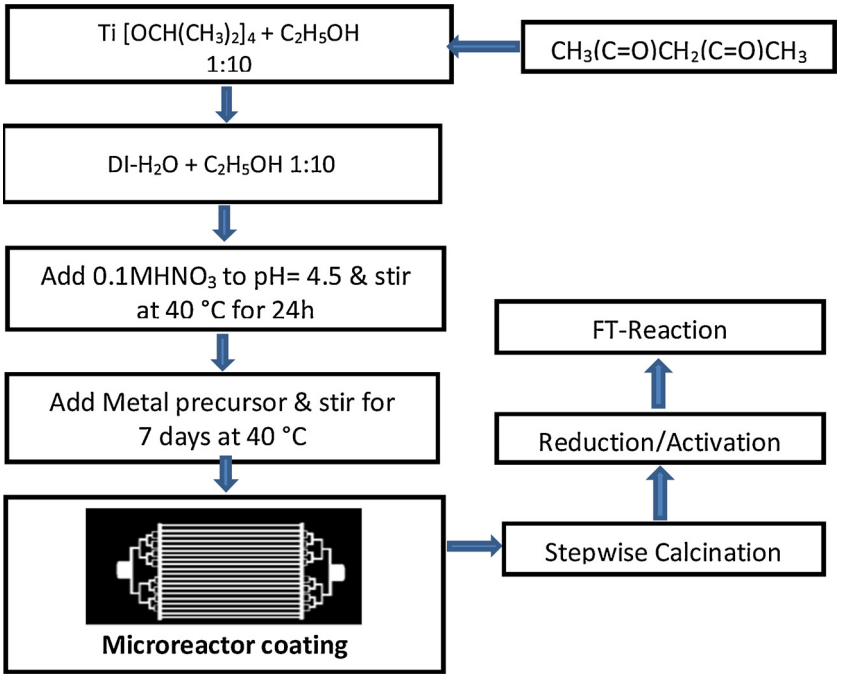

Fig. 1. Metal-TiO_2 sol-gel synthesis flow diagram.

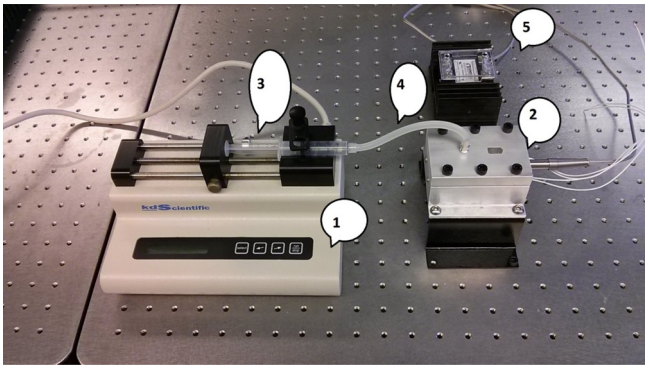

Fig. 2. CCI setup for catalyst coating (1) syringe pump; (2) aluminum heating block with microreactor inside; (3) syringe; (4) Si-tube; (5) solid state relay.

throughout the injection. When the first drop of sol-gel solution shows up at the outlet, the pump is turned off. Despite the fact that the CCI method is relatively more time-consuming, it is less complicated and cheaper than other coating methods [4]. The loaded microreactor is first dried at 450 °C for 24 h then dried at 100 °C for another 24 h and then calcined as discussed below.

The coated microreactors were calcined in a stepwise fashion at 200 °C for 1 h, 400 °C for 2 h and 500 °C for 4 h at a ramp rate of 4 °C/min. The stepwise heating is essential for the gradual decomposition or removal of the metal precursors and the stabilizer to minimize cracking of the coated surfaces. This ultimately makes the catalyst adhere better unto the silicon interface and it is suitable during the F-T reaction. Calcined microreactors and powder form of the catalysts (Table 1) were reduced under hydrogen/argon (10/90 vol ratio) atmosphere. The tubular furnace was first purged with nitrogen for 30 min in order to remove traces of air. The flow rate of the hydrogen/argon mixture was set at 3.5 L/min at a heating ramp rate of 5 °C/min. Table 1 shows the reduction conditions for the calcined powder and coated microreactor catalysts. *The hydrocarbon selectivity was quantified on carbon basis and CO_2 selectivity was not included in the calculations and the formulas are as follows:*

$$CO\ Conversion(\%) = \frac{molesof\ CO_{in} - moles\ of\ CO_{out}}{molesof\ CO_{in}}$$

$$CH_4\ Selectivity\ (\%) = \frac{mCH_4}{mCH_4 + 2mC_2H_6 + 3mC_3H_8 + 4mC_4H_{10}} \times 100$$

$$C_2H_6\ Selectivity\ (\%) = \frac{2mC_2H_6}{mCH_4 + 2m\ {}_2H_6 + 3mC_3H_8 + 4mC_4H_{10}} \times 100$$

We must emphasize that although CO_2 selectivity can be used as a descriptor of the water-gas–shift activity, it was not included in the calculations because our paramount objective was to understand the distinctive interaction between the TiO_2 support and the Fe, Co, Ru metals and how it differs from that observed in our previous study with SiO_2.

Fischer-Tropsch experimental set up and operation

Fischer-Tropsch experiments were carried out using an *in-house* experimental setup built with precise control on the operating conditions - temperature, pressure and flow rate. Fig. 3 shows the experimental setup on a buoyant optical table which serves as anti-vibration bench. The complete set-up for micro devices consist of 1: mass flow controllers for H_2 and CO gases; 2: closed stainless steel heating block; 3:pressure gauge; 4: N_2 mass flow controller for; 5:Gas chromatography; 6:CO gas detector; 7:syringe pump; 8: Aluminum block for microreactor coating; 9: solid state relay; 10: electrical connections;11:Mass spectrometer (GCMS); 12: opened stainless steel heating block; 13: stainless steel heating block with elastomer gasket; 14: calcined and reduced microreactor. The flow rates for the reactants were controlled by a pre-calibrated mass flow controller (Cole-Parmer) with a maximum flow range of 1 sccm at 40 psi pressure. The carrier gas (Pure Nitrogen) was used to pre-calibrate the carrier gas flow controller (Aalborg) with a maximum flow rate of 10 sccm.

Table 1
Catalysts Reduction Conditions.

Catalyst System	Temperature (°C)	Duration(hours) Powder Samples	Duration(hours) Microreactors
12%Ru-TiO_2	400	6	10
12%Fe-TiO_2	550	6	10
12%Co-TiO_2	550	6	10

As shown in Fig. 3, both microreactor and a gasket with inlet/outlet holes were sandwiched between two stainless steel blocks for heating; and tightened with a torque wrench (45 psi) to make the unit leak proof. Different gaskets (graphite, polymers, hard paper, etc.) were examined, and the most thermally stable elastomer was chosen. The bottom block had two 1/16th in. stainless steel interconnectors, one end of which connects the external 1/16th in. tubings and the other is bored into the steel block connecting to a capillary hole inside the block having the same dimensions as the microreactor inlet. Both steel blocks had cartridge heaters (one in the top block and two in the bottom) and were used to attain the optimum reaction temperature. Two K-type thermocouples were lodged in the bottom block to ensure that the temperature of the block is maintained at the required set point. The detailed design is shown in Fig. 3. During the reaction, H_2 and CO gases are flown through gas filter units, then, into two separate Cole Parmer® flowmeters (model number-32907-51 for both) and then into the outlet tubing of the flow meters are connected to single 1/16th-in. tubing. This 1/16th in. tubing serves as a pre-mixer of the gases prior to entering the reactor and is connected to the inlet interconnector of the steel heating block. The outlet tubing of the block is connected to a Cole Parmer® pressure gauge (model number-00314IS), which measures the pressure buildup in the line. The gauge is connected to a pressure safety valve-PSV-D (Aalborg-PSV-1) that regulates the pressure in the line. The outlet of the PSV-D valve is connected directly to the carrier gas (Nitrogen) line, also controlled by an Aalborg mass flow controller (model number-GFC17). Finally, the mixture of the carrier gas and reaction products are detected on-line by a calibrated GC (Agilent 7890B) equipped with a TCD and a mass spectrometer (Agilent MSD 5977A series). The calibration was performed with various calibration gas-mixtures and pure gases obtained from Air-Gas Company. The TCD was used for the analyses of H_2, N_2, CO, CO_2 and CH_4 while the mass spectrometer was used to analyze C_2H_6, C_3H_8 and C_4H_{10} fractions. All the mass flow rates and pressure controllers were regulated using a LabVIEW® program. In a typical F-T reaction, the pre-reduced microreactor is placed in the heating block so that the catalyst-coated side touches the base heating block. This ensures a perfect alignment of the holes (inlet & outlet) of the microreactor and the heating block to make the catalyst have a direct contact with the syngas. A graphite gasket (same size as the reactor) is gently placed on top of the reactor to prevent channeling of the reactant gases. The elastomer (Blue-Gard asbestos free gasket) is then used to seal the entire opening of the heating block and tightened with a torque wrench (at 45 psi) to make the entire reaction unit/block air-tight or leak proof.

Results and discussion

Characterization of the catalysts

SEM-EDX elemental analysis and mapping of catalysts

The experimental and the theoretical metal loadings in the catalysts of the coated calcined microreactors are shown in Table 2.

The uncoated microreactor was weighed and subtracted from the

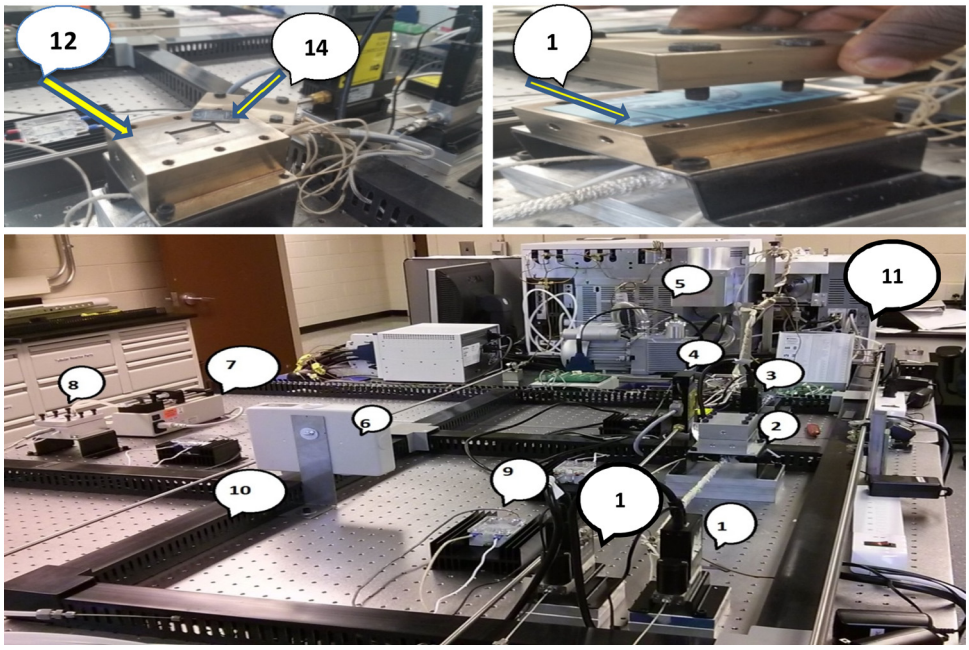

Fig. 3. Microreactor set up showing all microdevices on the optical Table.

Table 2
EDX Analysis of the Fe, Ru, and Co-TiO_2 Catalysts.

Catalyst	Intended loading (%)	Actual loading (%)
Fe/TiO_2	12	8.78
Co/TiO_2	12	8.34
Ru/TiO_2	12	6.44

weight of the microreactor after reduction. The average catalyst weight was found to be 0.5966 mg. The SEM image and the EDX analysis (Fig. 4) show that the 1.3 cm long × 50 µm wide × 100 µm deep microreactors were well coated, confirming the effectiveness of the CCI [30] approach described previously. The EDX elemental analysis further indicated that Co, Ru and Fe were uniformly embedded in the microchannels.

Thermogravimetric analysis-differential scanning calorimetry (TGA-DSC)

As-synthesized powder samples were subjected to simultaneous TGA-DSC studies to monitor their thermal decomposition behavior. Fig. 5 shows TGA profiles of all three catalysts. The endothermic weight loss below 100 °C is attributed to removal of moisture, ethanol and/or ethanol-isopropyl alcohol mixture formed during hydrolysis of the limiting reagent, TIP. The intense exothermic decomposition from 200 °C to 400 °C observed in all catalysts could be ascribed to decomposition of acetylacetonate-metal [$Co(acac)_2$, $Fe(acac)_2$, $Ru(acac)_2$] complexes as well as $TiO(acac)_2$ [33,34] species. This is consistent with the reports in literature that acetylacetonate (a bidentate β-diketonate ligand) binds to transition metals through its oxygen atoms to form stable chelates [35–37] that decomposes at relatively high temperature. The small weight loss between 400 °C and 600 °C is probably due to the removal of traces of acetic acid possibly produced from acetylacetonate decomposition. The phase change that occurred above 600 °C with negligible weight loss is associated with poly condensation of Ti—OH

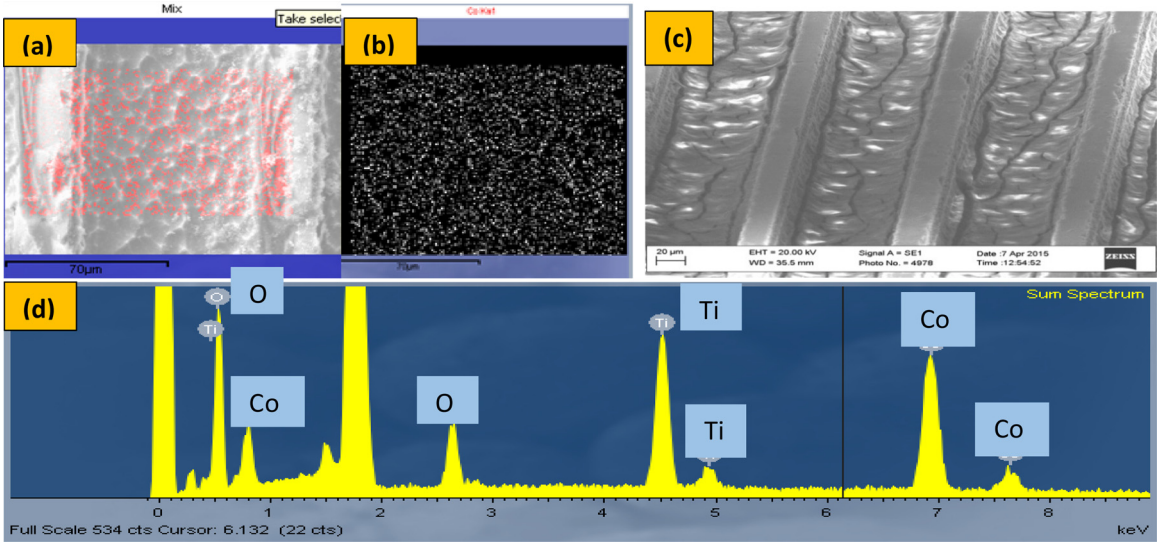

Fig. 4. SEM and EDX Analysis of calcined 12%Co-TiO_2 in Si-microreactor (a) elemental mapping (b) Particles distribution of TiO_2 support c) SEM image of coated microchannels and (d) elemental spectrum.

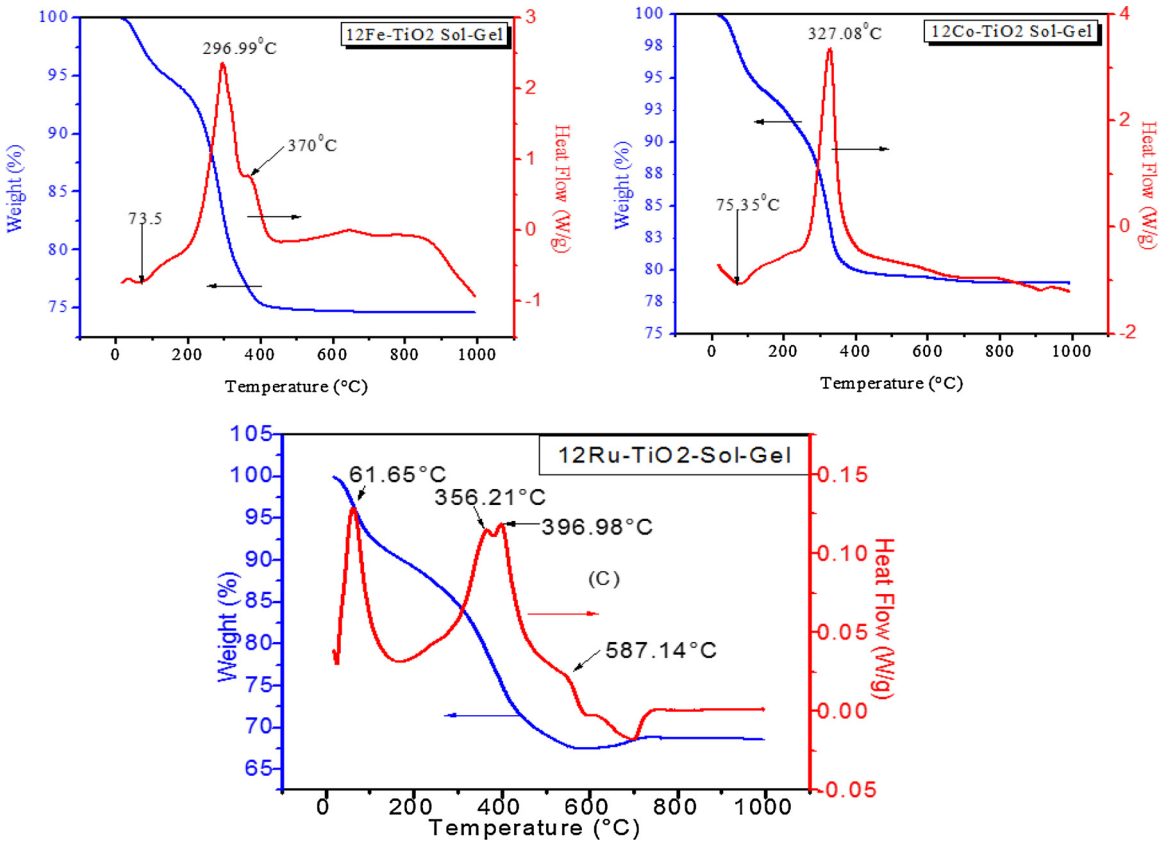

Fig. 5. TGA and DSC profiles of TiO_2 supported Co, Fe, and Ru catalysts used for F-T reactions.

groups to form the crystalline —Ti—O—Ti—O—Ti—O— anatase framework. [38]

Powder X-ray analysis

Fig. 6 shows wide angle X-ray diffraction (WAXRD) patterns of calcined catalysts. All three catalysts exhibited clearly defined intense peaks confirming their crystalline nature.12 wt% Fe-TiO_2 showed strong diffraction peaks at 25.2°,37.8°,48.1°,54.5°, and 62.6° indexed at (101), (004), (200), (211) and (204) reflection planes respectively; indicative of the anatase phase of TiO_2. [39]. The anatase structure of 12 wt% Co-TiO_2 is also confirmed by the diffraction peaks at 2θ values of 25.3°, 36.8°, 37.8°, 48°, 53.9°, 55°, and 62.6° indexed to the (101), (103), (004), (200), (105), (211), (204) planes respectively. [39,40] 12 wt% Ru-TiO_2 showed diffraction peaks 25.19°,27.48°, 34.93°,

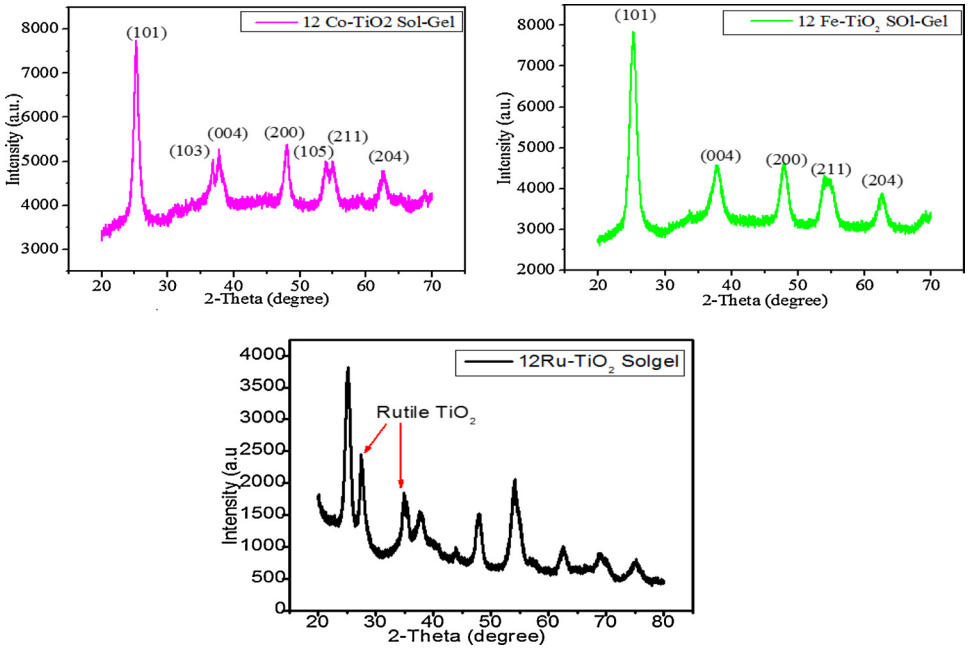

Fig. 6. Powder X-ray diffraction patterns of TiO_2 supported Co, Fe and Ru catalysts.

Table 3
Surface Area, Pore Size, and Pore Volume of Calcined Catalysts.

Catalyst System	Surface Area (m^2/g)	Average pore size (nm)	Pore Volume (cc/g)
12%Ru-TiO_2	118.39	4.75	0.19
12%Fe-TiO_2	117.03	5.85	0.25
12%Co-TiO_2	48.15	3.62	0.07

37.83°, 47.46°, 53.91°, 62.83°, 68.84°, and 75.1°. No discernible peaks observed for the metal oxides suggested that either the metal oxides are not crystalline enough compared to TiO_2 (i.e., relatively weaker diffractions)or well dispersed on the surface. [41,42] The intense peaks at 27.48^0 and 34.93 Ru-TiO_2 in Fig. 6 are indexed to 110 plane of the rutile phase of TiO_2 [43,44]. These peaks suggest that unlike Fe and Co, Ru-TiO_2 sol-gel consists of mixed anatase and rutile phases of TiO_2.

The size of TiO_2 crystallites calculated by the Scherer equation were 6.91 nm, 8.27 nm and 9.9 nm for Fe-TiO_2 Ru-TiO_2, and Co-TiO_2 catalysts, respectively

Surface area analysis of calcined samples

The specific surface area, pore-size, and pore volume of the catalysts were determined using a Quantachrome NOVA 2200e instrument. Adsorption-desorption isotherms were generated by flowing nitrogen onto the material in a bath of liquid nitrogen at 77 K. Prior to analysis, the samples were degassed under vacuum at 150 °C. The surface area was calculated by using Brunauer-Emmett-Teller (BET) equation from the adsorption branch of the isotherm in a relative pressure (P/P_0) range of 0.07–0.3. The total pore volume was derived based on the amount of N_2 adsorbed at a relative pressure close to unity. Table 3 summarizes the multipoint BET analyses of the powder form of calcined catalysts. The average pore sizes suggested mesoporosity of the nano-catalysts.

H_2-temperature programmed reduction (TPR) analysis

Fig. 7 shows the reduction profiles of the calcined powder catalysts. The profiles clearly show that the interaction with TiO_2 was different for each metal. Unlike Co-TiO_2 and Fe-TiO_2, Ru-TiO_2 was reduced at relatively lower temperature from 100 °C to about 240 °C. The main hydrogen consumption from 80 °C to 125 °C is associated with the reduction of Ru^{3+} to Ru^0. The reduction from 150 °C to 250 °C is ascribed to ruthenium oxides with strong intimacy with the TiO_2 support and/or possible ruthenium oxychlorides formed during the catalysts synthesis [45].The reduction profile of Fe/TiO_2 occurred in three steps. The first peak at 330 °C corresponds to reduction of Fe_2O_3, while Fe_3O_4 and FeO were reduced around 450 °C and 800 °C respectively [46–48]. Reduction of Co-TiO_2 occurred in two steps. The first hydrogen uptake around 350 °C is associated with the reduction of Co_3O_4 to CoO. The second peak that begins around 400 °C, centered at 530 °C and end around 700 °C is ascribed to the reduction of CoO to Co as well as reduction of cobalt-titanate mixed supports which are very difficult to reduce. [49,50]. The impact of the ease of metal oxides reduction/activation on F-T activity is discussed on page 22.

Fischer-Tropsch (F-T) studies in Si-microreactor)

The effect of reaction temperature (150 °C, 180 °C, 220 °C, 250 °C and 300 °C) on the catalytic performance of 12%Co-TiO_2, 12%Fe-TiO_2 and 12%Ru-TiO_2 were investigated to ascertain the optimum reaction temperature in terms of CO conversion and hydrocarbon selectivity for each catalyst. Prior to each reaction, the pre-reduced microreactors were reduced with H_2 in-situ at 300 °C for 2 h. The H_2/CO molar ratio was set constant at 2/1 at a total flow rate of 0.6 ml/min. The flow rate of N_2 (internal standard) and total reaction pressure was set at 1 ml/min and 1.0 atm respectively for all reactions.

As shown in Fig. 8, for 12%Co-TiO_2, no CO conversion was observed at 150 °C and 180 °C. Surprisingly, after 1 h of reaction the catalysts deactivated rapidly except at 220 °C. Within 30 min after the reaction started, CO conversion was 68% at 220 °C then declined to ~32% after 2 h followed by complete loss of activity. In contrast, at 250 °C and 300 °C the catalyst initially attained a CO conversion of ~100% and 89% respectively, but deactivated completely after 1 h. A temperature increase did not seem to have any significant effect on hydrocarbon selectivity. Methane selectivity was ≥95% in the temperature range of 220 °C–300 °C. While the ethane selectivity capped at 4% at 250 °C, no C_3/C_4 products were detected at any reaction temperature. These results are significantly different from that reported previously for F-T studies using Co-SiO_2 catalysts in a Si-microreactor. In our previous studies, CO conversion more than 90% with a selectivity to propane, ethane and methane in the order Co > Fe > Ru with SiO_2 support were observed. More significantly, deactivation studies showed that Co-SiO_2 was stable for a long period of time, for more than 70 h.

The activity of the catalyst with TiO_2 support depends on the crystalline structure of support. In order to understand this behavior of Co-TiO_2, especially instability of the catalyst for FT synthesis in microreactor, we looked closely at the XRD of Co-TiO_2 and TPR results and compared them to that reported in the literature. As described above in the XRD section, Co-TiO_2 predominantly shows the crystalline form of anatase. Jongsomjit et al., reported that the activity of the catalyst with rutile phase in TiO_2 for Co based catalyst greatly enhanced activity during CO hydrogenation. This rutile phase in titania favors reduction of Co oxides into cobalt metal [51]. It is also reported to enhance the stability of the titania support leading to lesser degrees of loss in reducibility during the reduction of catalyst. Previous studies have shown that around 15% of rutile phase in TiO_2 exhibited four times higher conversion rate than that of pure anatase, TiO_2 [22,24]. Thus, the absence of any appreciable amount of rutile phase in TiO_2 of our sol-gel supported catalysts may explain why the Fe and Co catalysts lost their activity in a short time, culminating in a rapid decline of CO conversion.

As shown in Fig. 9, the overall trend for CO conversion using 12% Fe-TiO_2 was similar to that of 12%Co-TiO_2.

Nonetheless few subtle distinctions are worth pointing out. A significant CO hydrogenation, 85% and 73%, was observed at 180 °C and 150 °C respectively within 30 min of reaction. A sharp decline in deactivation was observed at all reaction temperatures. Interestingly, whereas Cobalt displayed 100% CO at 250 °C, iron performed poorly (~8%) at the same temperature. In contrast, while complete deactivation of Co at 300 °C, occurred after 2 h, Fe maintained, ~23% CO conversion after 4 h at the same temperature. Although 100% methane selectivity was sustained as temperature was increased from 150 °C to 250 °C, no selectivity towards C_2-C_4 products was observed. At higher temperature - 300 °C, 12%Fe-TiO_2 performed much better with selectivity of ~80%, ~7%,11.6% and ~4% towards methane, ethane, propane and butane respectively. Conspicuously, as the temperature was increased from 250 °C to 300 °C, Fe-TiO_2 regained activity with ~ 20% increase in CO conversion. Concomitantly, −CH− chain growth was enhanced producing relatively more hydrocarbons (C_2-C_4) as well as traces of oxygenates. We believe that transformation of the iron oxides/FeO to iron carbide (between 250 °C and 300 °C) was responsible for the improvement in the activity of Fe-TiO_2. This behavior is in good agreement with observations made by Ordomsky et al [52].They reported that carbidization of iron occurred after treatment with CO at 350 °C for 4 h followed by syngas purging at 300 °C for 2 h. They inferred that the presence of carbon in iron carbide lattices enhanced CO hydrogenation to methane and initiated chain growth reactions leading to formation of C_2-C_4 hydrocarbons. The higher stability and reactivity of iron carbide phase of iron catalysts relative to that of oxides are consistent with that reported by other research groups. [53,54]

Fig. 10 shows CO conversion for 12%Ru-TiO_2 (except at 150 °C) that is sharply different from those observed for Co and Fe. Although the rate of 12%Ru-TiO_2 deactivation at 220 °C was faster than the rate at

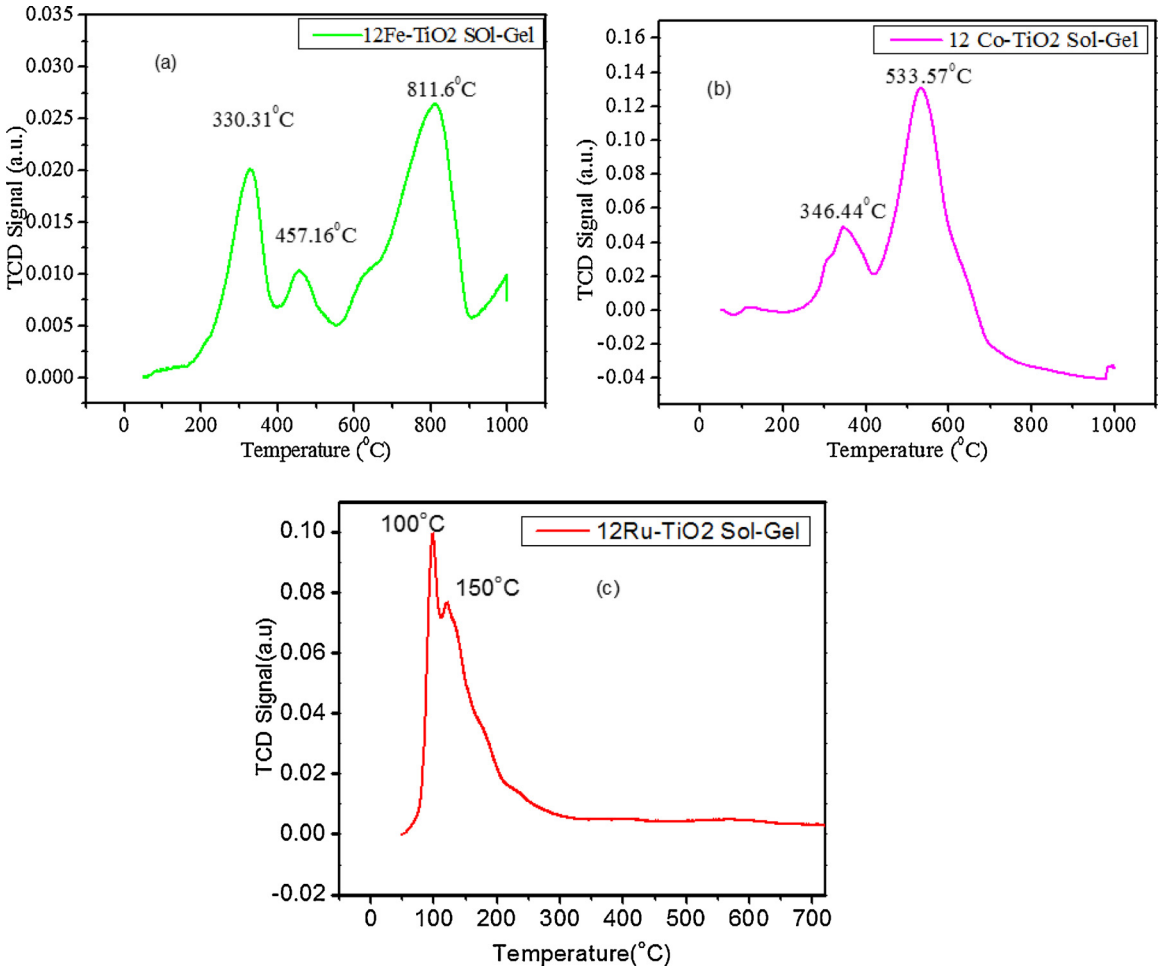

Fig. 7. Temperature Programmed Reduction profiles of TiO_2 supported Co, Fe and Ru catalysts with hydrogen (H_2).

180 °C, both Fe and Co catalysts were completely deactivated after 5 h. The Ru catalyst stability improved with increasing temperature. At the end of 1 h time-on-stream, CO conversion was 100% at all temperatures except at 150 °C. At 180 °C, CO conversion was 100% for 4 h and then deactivated steadily to˜80% an hour later. At 220 °C, gradual deactivation began after 2 h, and CO conversion decreased from 98% to about 74% after 5 h. CO conversion at 250 °C increased sharply (within 30 min of reaction) from ˜60% to 100% after 1 h and held steady after 7 h. The reaction at 300 °C, started with 100% CO conversion and remained the same after 7 h, showed no sign of deactivation similar to the reaction at 250 °C.

In addition to better CO conversion and stability, 12%Ru-TiO_2 also showed relatively higher selectivity towards C_1-C_4 hydrocarbons. As expected, when CH_4 selectivity increased, selectivity towards the other hydrocarbons decreased and vice versa. Increasing temperature did not have a definitive pattern/trend on the hydrocarbon selectivity. CH_4 selectivity was 90% at 150 °C, decreased monotonically to 49% at 220 °C, and then increased rapidly to 100% at 300 °C. At 150 °C, selectivity towards ethane, propane and butane was 2.9%, 3.7% and 2.5% respectively when steady state was reached. When temperature was increased to 180 °C, selectivity rose slightly to ethane 4.9%, and ˜8% for both propane and butane. Reaction at 220 °C yielded the highest C_2-C_4 hydrocarbon selectivity- ˜11% ethane, 22% propane and ˜17% butane. The selectivity at 250 °C declined to ˜6% ethane, 5% propane and 2% butane. However, unlike 12%Fe-TiO_2, selectivity of 12%Ru-TiO_2 towards all the C_2-C_4 hydrocarbons was not significant at 300 °C. This

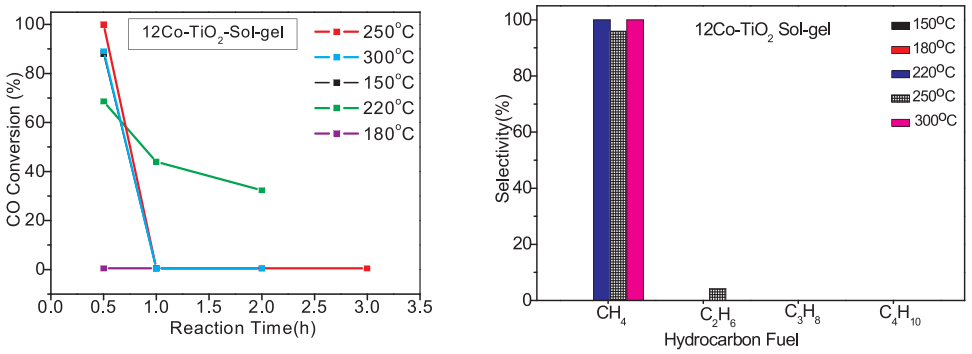

Fig. 8. Effect of temperature on CO conversion (left) and hydrocarbon selectivity (right) of 12%Co-TiO_2 catalyst.

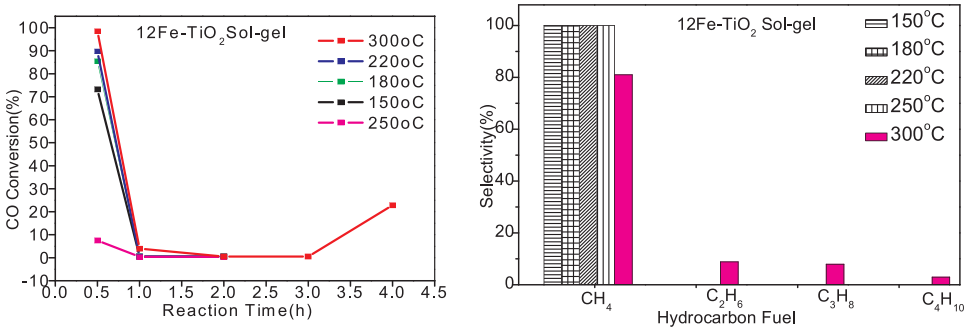

Fig. 9. Effect of temperature on CO conversion (left) and hydrocarbon selectivity (right) of 12%Fe-TiO_2 catalyst.

suggested that at 300 °C, absolutely no −CH− polymerization took place and the Ru (F-T) activity was mainly methanation of CO. The dominant C_2-C_4 selectivity of 12%Ru-TiO_2 compared to12%Fe-TiO_2 and12%Co-TiO_2 is in sound agreement with observations made by Gonzalez Carballo and coworkers [55]. They reported that at 250 °C CO dissociation sites of Ru-TiO_2 are readily available at the initial stages of reaction, thereby forming numerous C_1 moieties which upon hydrogenation diffuse rapidly to the chain growth sites to promote formation of higher hydrocarbons.

Currently, the molecular/atomic level mechanism for the rapid deactivation of Fe-TiO_2 and Co-TiO_2 especially that of Co-TiO_2 catalysts are not fully understood. In our previous study, Fe, Co and Ru supported on SiO_2 showed very good stability in the order of Co-SiO_2 > Fe-SiO_2 > > Ru-SiO_2 [30]. Our current results suggest that the type of support and the crystalline phase of TiO_2 have a profound effect on the F-T activity of the catalysts. Jongsomjit et al, [56,57] as well as Shimura and coworkers [22] have shown that for TiO_2 supported catalysts, the greater the rutile to anatase crystal phase ratio (19% Rutile yields optimum performance) in the TiO_2 crystal lattice, better stability and F-T activity are observed. As discussed previously in our WAXRD analysis (Fig. 6), only 12%Ru-TiO_2 exhibited a rutile crystal polymorph. This indicated that under our reaction conditions, the mixed rutile and anatase crystal phases played a major role in the catalytic stability and superiority of 12%Ru-TiO_2. The rutile phase in the support undoubtedly enhanced the FT synthesis. Furthermore, the very low reduction/activation temperature of the ruthenium oxides (80 °C–200 °C) also contributed to its better reactivity. Hurst and coworkers [60] elucidated that the lower the reduction temperature (greater ease of reduction) the more negative is the Gibbs free energy (ΔG) of the reduction process and the greater the reactivity of the metal. They also ascertained that the ease of reducibility promotes an optimum metal support interaction which results in an enhanced dispersion of the metal active sites. Conversely, the dominant TiO_2 anatase phase in 12%Fe-TiO_2 and 12%Co-TiO_2 may have played a significant role in their rapid deactivation and poor F-T performance especially in the case of 12%Co-TiO_2. In the case of Fe-TiO_2, formation of Fe-carbide is important and provides stability and conversion of CO. The chemical properties especially of TiO_2 as a catalyst mainly depend on the anatase and rutile phase fractions of the material. Thus, changing reaction conditions to favor a rutile phase of TiO_2 can significantly enhance the performance of the catalyst. In addition, the calcination temperature, relative ease of reducibility of the metal oxides and interaction with the type of active crystal phase of the metal oxides could also be a factor in the catalyst's performance. Shimura et al concluded that Co/TiO_2 exhibits strong metal support interaction (SMSI) hence minimizes the aggregation of the Co active sites during H_2-reduction, resulting in decreased Co metal dispersion and low FT activity. Their observation which is underscored by ours suggests that the high temperature reduction profiles of Fe-TiO_2 and Co-TiO_2 (Fig. 7) play an important role; they indicate that SMSI could have been a factor in the poor FT activity of both catalysts. Diehl et al. [58] pointed out that decrease in cobalt particle sizes to about 6–8 nm results in higher methane selectivity and Almeida et al [59] concluded that the catalyst layer in microchannels must be optimized to establish a porosity domain that permits easy diffusion of the feed (syngas) through the pores of the catalyst coating and particles. The latter group showed that increase in thickness of catalyst coating (from 32um to 82um) augments the resistance to diffusion of CO gas which leads to quick deactivation and profoundly affect the hydrocarbon selectivity as well as productivity per unit volume of the reactor.

Conclusion

Silicon based microchannel microreactors were used for Fischer-Tropsch studies with Fe, Co and Ru as catalyst on TiO_2 sol-gel support to understand the interaction of support with metal. The uniform coating inside the microchannels was obtained using the closed channel infiltration method. XRD and TPR studies indicated the presence of mixed rutile and anatase polymorphs in Ru-TiO_2. In contrast, only the anatase phase was present in the Co-TiO_2 and Fe-TiO_2 catalysts. The rultile phase of Ru-TiO_2 played a significant role on CO conversion under the operating conditions at 1 atm in the temperature range of 150 °C–300 °C. Unlike Ru-TiO_2 which was reduced at a quite lower

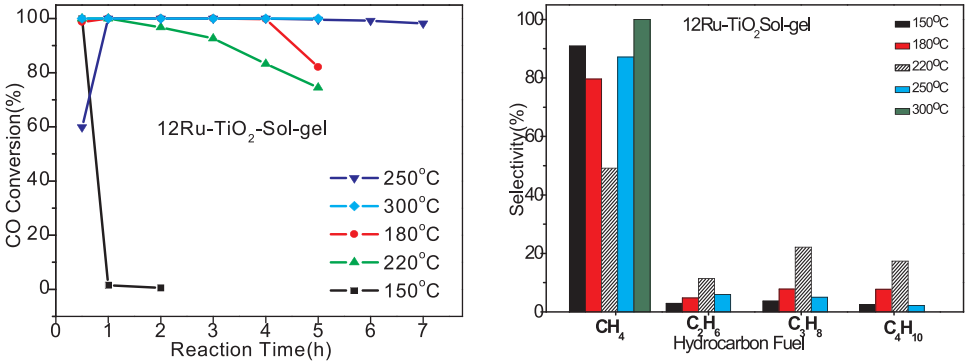

Fig. 10. Effect of temperature on CO conversion (left) and hydrocarbon selectivity (right) of 12%Ru-TiO_2 catalyst.

temperature, the high temperature reduction profiles of Fe-TiO_2 and Co-TiO_2 indicated a significant strong metal (Co and Fe) support interaction (SMSI). This most likely caused a minimal dispersion of the metal active sites that could be a major factor in the poor FT activity of both Fe- and Co-catalysts. In regard to hydrocarbon selectivity and stability of the catalyst, the optimum reaction temperature for 12%Co-TiO_2 was 220 °C while for 12%Fe-TiO_2 it was 300 °C. Unlike Ru-TiO_2, the absence of significant amount of rutile polymorph in Co-TiO_2 and Fe-TiO_2 decreased the stability and selectivity of the catalysts. In the case of 12%Ru-TiO_2, although CO conversion was similar at 220 °C and 250 °C, C_2-C_4 selectivity was much higher at 220 °C than that observed at 250 °C. However, due to better catalyst stability at 250 °C, it was chosen as the optimum reaction temperature for 12%Ru-TiO_2. In overall, both catalysts stability and reactivity were in the order 12%Ru-TiO_2 > > 12%Fe-TiO_2 > 12%Co-TiO_2. These results are significantly different from our previous work with silica wherein stability was in the order of Co-SiO_2 > Fe-SiO_2 > > Ru SiO_2.

Acknowledgements

The authors acknowledge the funding received from National Science Foundation (NSF) for the NSF-CREST Bioenergy Center (Grant No. HRD-124215). The authors thank Dr. Tashfin Hossain and Nafeezudin Mohammad for their help with this manuscript. The authors would like to thank Dr. Shamsuddin Ilias for the use of his BET set-up for surface analysis and Dr. Lijun Wang for use of his Chemical Analyzer for TPR studies. The authors would like to thank Mr. Bryce Holmes (School of Agriculture and Environmental Sciences) and Mr. James King (Chemistry Department) for their support with the experimental work. The authors thank Dr. Sankar and Dr. Yarmolenko (Center for Advanced Materials and Smart Structures-CAMSS) at NCAT for the use of XRD for material characterization. Finally, we acknowledge the Joint School of Nanoscience and Nanoengineering (JSNN) for help acquiring the data using the TEM and SEM-EDX instruments.

References

[1] D. Leckel, Diesel production from Fischer – Tropsch: the past, the present, and new concepts, Energy Fuels 23 (2009) 2342–2358.
[2] Johannesburg, Project Update: Oryx Gas-to-Liquids (GTL) Joint Venture, (2007) sasol.com.
[3] A.L. Tonkovich, T. Mazanec, K. Jarosch, S. Fitzgerald, B. Yang, Gas-to-Liquids Conversion of Associated Gas Enabled by Microchannel Technology, (2009), pp. 1–7 Velocys.com.
[4] S. Mehta, Comparative Studies of Silica Sol-Gel Supported Iron, Cobalt and Ruthenium Catalysts for Fischer-Tropsch Reaction in Microreactorrs, Chemical Engineering, Louisiana Tech University, 2006.
[5] J.J. Lerou, A.L. Tonkovich, L. Silva, S. Perry, J. McDaniel, Microchannel reactor architecture enables greener processes, Chem. Eng. Sci. 65 (2010) 380–385.
[6] V.S. Nagineni, Sol-Gel Encapsulated Catalysts for Synthesis Gas Conversion to Higher Alkanes in a Microreactor, Louisiana Tech University, 2004.
[7] P. Norberg, L. Patersson, I. Lundström, Characterization of gas transport through micromachined submicron channels in silicon, Vacuum 45 (1994) 139–144.
[8] A.M. Thayer, Harnessing Microreactors vol. 83, Chemical and Engineering News, 2005, pp. 43–52.
[9] M. Guglielmi, G. Carturan, Precursors for sol-gel preparations, J. Non-Cryst. Solids 100 (1988) 16–30.
[10] L. Y, Development of a Novel Microreactor for Improved Chemical Reaction Conversion, Louisiana Tech University (IfM), 2005.
[11] B.G. Johnson, C.H. Bartholomew, D.W. Goodman, The role of surface structure and dispersion in CO hydrogenation on cobalt, J. Catal. 128 (1991) 231–247.
[12] H. Schmidt, Chemistry of material preparation by the sol-gel process, J. Non-Cryst. Solids 100 (1988) 51–64.
[13] V. Mazzieri, F. Coloma-Pascual, A. Arcoya, P. L'Argentière, N. Fí, XPS, FTIR and TPR characterization of Ru/Al_2O_3 catalysts, Appl. Surf. Sci. 210 (2003) 222–230.
[14] P. Norberg, L.G. Patersson, I. Lundström, Characterization of gas transport through micromachined submicron channels in silicon, Vacuum 45 (1994) 139–144.
[15] L. Wei, Y. Zhao, Y. Zhang, C. Liu, J. Hong, H. Xiong, J. Li, Fischer–Tropsch synthesis over a 3D foamed MCF silica support: toward a more open porous network of cobalt catalysts, J. Catal. 340 (2016) 205–218.
[16] A.M. Venezia, V. La Parola, L.F. Liotta, G. Pantaleo, M. Lualdi, M. Boutonnet, S. Järås, Co/SiO2 catalysts for Fischer–Tropsch synthesis; effect of Co loading and support modification by TiO2, Catal. Today 197 (2012) 18–23.
[17] Y.-H. Zhao, C. Liu, Y.-H. Song, Q.-J. Zhang, M.-L. Zhu, Z.-T. Liu, Z.-W. Liu, Direct synthesis of the reduced Co–C/SiO2 as an efficient catalyst for Fischer–Tropsch synthesis, Ind. Eng. Chem. Res. 57 (2018) 1137–1145.
[18] M. Dad, R.J. Lancee, M. Janse van Vuuren, J. van de Loosdrecht, J.W.H. Niemantsverdriet, H.O.A. Fredriksson, SiO2 -supported Fe & FeMn colloids—Fischer-Tropsch synthesis on 3D model catalysts, Appl. Catal. A Gen. 537 (2017) 83–92.
[19] J. Zhang, J. Chen, J. Ren, Y. Sun, Chemical treatment of γ-Al2O3 and its influence on the properties of Co-based catalysts for Fischer–Tropsch synthesis, Appl. Catal. A Gen. 243 (2003) 121–133.
[20] G. Jacobs, T.K. Das, P.M. Patterson, J. Li, L. Sanchez, B.H. Davis, Fischer–Tropsch synthesis XAFS, Appl. Catal. A Gen. 247 (2003) 335–343.
[21] T.O. Eschemann, K.P. de Jong, Deactivation behavior of Co/TiO2 catalysts during Fischer–Tropsch synthesis, ACS Catal. 5 (2015) 3181–3188.
[22] K. Shimura, T. Miyazawa, T. Hanaoka, S. Hirata, Fischer–Tropsch synthesis over TiO2 supported cobalt catalyst: effect of TiO2 crystal phase and metal ion loading, Appl. Catal. A Gen. 460–461 (2013) 8–14.
[23] C. Liu, Y. He, L. Wei, Y. Zhang, Y. Zhao, J. Hong, S. Chen, L. Wang, J. Li, Hydrothermal carbon-coated TiO2 as support for Co-based catalyst in Fischer–Tropsch synthesis, ACS Catal. 8 (2018) 1591–1600.
[24] Y.W. Chen, H.T. Wang, J.G. Goodwin, Effect of preparation methods on the catalytic properties of zeolite-supported ruthenium in the Fischer-Tropsch synthesis, J. Catal. 83 (1983) 415–427.
[25] Y.W. Chen, H.T. Wang, J.G. Goodwin, W.K. Shiflett, Fischer-Tropsch synthesis over zeolite-supported ruthenium catalysts derived from Ru3(CO)12, Appl. Catal. 8 (1983) 303–314.
[26] S.-H. Kang, J.W. Bae, P.S. Sai Prasad, K.-W. Jun, Fischer–Tropsch synthesis using zeolite-supported Iron catalysts for the production of light hydrocarbons, Catal. Lett. 125 (2008) 264.
[27] K. Jothimurugesan, S. Gangwal, Titania-supported bimetallic catalysts combined with HZSM-5 for Fischer – Tropsch synthesis, Ind. Eng. Chem. Res. 37 (1998) 1181–1188.
[28] D.J. Duvenhage, N.J. Coville, Fe:Co/TiO2 bimetallic catalysts for the Fischer–Tropsch reaction: Part 2. The effect of calcination and reduction temperature, Appl. Catal. A Gen. 233 (2002) 63–75.
[29] D.J. Duvenhage, N. Coville, Fe:Co/TiO2 Bimetallic Catalysts for the Fischer–Tropsch Reaction: Part 4: a Study of Nitrate and Carbonyl Derived FT Catalysts, (2005).
[30] S. Mehta, V. Deshmane, S. Zhao, D. Kuila, Comparative studies of silica-encapsulated iron, cobalt, and ruthenium nanocatalysts for Fischer–Tropsch synthesis in silicon-microchannel microreactors, Ind. Eng. Chem. Res. 53 (2014) 16245–16253.
[31] S. Zhao, Nano Scale Platinum and Iron-Cobalt Catalysts Deposited in Microchannel Microreactors for Use in Hydrogenation and Dehydrogenation of Cyclohexane Selective Oxidation of Carbon Monoxide and Fischer-Tropsch Process to Higher Alkanes, Louisiana Tech University(IfM), 2003.
[32] K. Haas-Santo, M. Fichtner, K. Schubert, Preparation of microstructure compatible porous supports by sol–gel synthesis for catalyst coatings, Appl. Catal. A Gen. 220 (2001) 79–92.
[33] N. Papadopoulos, E. ILLEKOVA, H. Karayanni, E. Hristoforou, Synthesis and characterization of cobalt precursors for the growth of magnetic thin films by the MOCVD method, J. Optoelectron. Adv. Mater. 10 (2008) 1098–1102.
[34] I.O. Acik, J. Madarász, M. Krunks, K. Tõnsuaadu, G. Pokol, L. Niinistö, Titanium (IV) acetylacetonate xerogels for processing titania films, J. Therm. Anal. Calorim. 97 (2009) 39–45.
[35] C. Wai, S. Wang, Separation of metal chelates and organometallic compounds by SFC and SFE/GC, J. Biochem. Biophys. Methods 43 (2000) 273–293.
[36] T. Oshiki, H. Yamashita, K. Sawada, M. Utsunomiya, K. Takahashi, K. Takai, Dramatic rate acceleration by a diphenyl-2-pyridylphosphine ligand in the hydration of nitriles catalyzed by Ru (acac) 2 complexes, Organometallics 24 (2005) 6287–6290.
[37] Z. Czech, M. Wojciechowicz, The crosslinking reaction of acrylic PSA using chelate metal acetylacetonates, Eur. Polym. J. 42 (2006) 2153–2160.
[38] S. Janitabar Darzi, A.R. Mahjoub, A. Nilchi, Synthesis of spongelike mesoporous anatase and its photocatalytic properties, Iran. J. Chem. Chem. Eng. 29 (2010).
[39] S.K. Das, M.K. Bhunia, A. Bhaumik, Self-assembled TiO2 nanoparticles: mesoporosity, optical and catalytic properties, J. Chem. Soc. Dalton Trans. 39 (2010) 4382–4390.
[40] K. Baiju, P. Shajesh, W. Wunderlich, P. Mukundan, S.R. Kumar, K. Warrier, Effect of tantalum addition on anatase phase stability and photoactivity of aqueous sol–gel derived mesoporous titania, J. Mol. Catal. A Chem. 276 (2007) 41–46.
[41] H. Zhu, Z. Qin, W. Shan, W. Shen, J. Wang, Pd/CeO 2–TiO2 catalyst for CO oxidation at low temperature: a TPR study with H2 and CO as reducing agents, J. Catal. 225 (2004) 267–277.
[42] L. Deng, S. Wang, D. Liu, B. Zhu, W. Huang, S. Wu, S. Zhang, Synthesis, characterization of Fe-doped TiO2 nanotubes with high photocatalytic activity, Catal. Lett. 129 (2009) 513–518.
[43] G. Kavei, A. Nakaruk, C.C. Sorrell, Equilibrium state of anatase to rutile transformation for titanium dioxide film prepared by ultrasonic spray pyrolysis technique, Mater. Sci. Appl. 2 (2011) 700.
[44] Z. Liu, X. Zhang, S. Nishimoto, M. Jin, D.A. Tryk, T. Murakami, A. Fujishima, Anatase TiO2 nanoparticles on rutile TiO2 nanorods: a heterogeneous nanostructure via layer-by-layer assembly, Langmuir 23 (2007) 10916–10919.
[45] V.P. Kumar, Y. Harikrishna, N. Nagaraju, K.V. Chary, Characterization and reactivity of TiO2 supported nano ruthenium catalysts for vapour phase hydrogenolysis of glycerol, Indian J. Chem. Sect. A-Inorg. Bio-Inorg. Phys. Theor. Anal. Chem. 53 (2014) 516–523.

[46] G. Munteanu, L. Ilieva, D. Andreeva, Kinetic parameters obtained from TPR data for α-Fe 2O3 and Auα-Fe2O3 systems, Thermochim. Acta 291 (1997) 171–177.
[47] G. Neri, A. Visco, S. Galvagno, A. Donato, M. Panzalorto, Au/iron oxide catalysts: temperature programmed reduction and X-ray diffraction characterization, Thermochim. Acta 329 (1999) 39–46.
[48] S. Minicò, S. Scirè, C. Crisafulli, R. Maggiore, S. Galvagno, Catalytic combustion of volatile organic compounds on gold/iron oxide catalysts, Appl. Catal. B 28 (2000) 245–251.
[49] J.-H. Oh, J.W. Bae, S.-J. Park, P. Khanna, K.-W. Jun, Slurry-phase Fischer–Tropsch synthesis using Co/γ-Al2O3, Co/SiO2 and Co/TiO2: effect of support on catalyst aggregation, Catal. Lett. 130 (2009) 403–409.
[50] M. Feyzi, S. Nadri, M. Joshaghani, Catalytic performance of Fe-Mn/Si nanocatalysts for CO hydrogenation, J. Chem. 2013 (2012).
[51] D.J. Duvenhage, N.J. Coville, Fe:Co/TiO2 bimetallic catalysts for the Fischer–Tropsch reaction: part 4: a study of nitrate and carbonyl derived FT catalysts, J. Mol. Catal. A Chem. 235 (2005) 230–239.
[52] V. Ordomsky, B. Legras, K. Cheng, S. Paul, A. Khodakov, The role of carbon atoms of supported iron carbides in Fischer–Tropsch synthesis, Catal. Sci. Technol. 5 (2015) 1433–1437.
[53] D.H. Chun, J.C. Park, S.Y. Hong, J.T. Lim, C.S. Kim, H.-T. Lee, J.-I. Yang, S. Hong, H. Jung, Highly selective iron-based Fischer–Tropsch catalysts activated by CO2-containing syngas, J. Catal. 317 (2014) 135–143.
[54] E. de Smit, F. Cinquini, A.M. Beale, O.V. Safonova, W. van Beek, P. Sautet, B.M. Weckhuysen, Stability and reactivity of ε− χ− θ iron carbide catalyst phases in Fischer− Tropsch synthesis: controlling μC, J. Am. Chem. Soc. 132 (2010) 14928–14941.
[55] J.M.G. Carballo, E. Finocchio, S. García-Rodriguez, M. Ojeda, J.L.G. Fierro, G. Busca, S. Rojas, Insights into the deactivation and reactivation of Ru/TiO2 during Fischer–Tropsch synthesis, Catal. Today 214 (2013) 2–11.
[56] B. Jongsomjit, T. Wongsalee, P. Praserthdam, Characteristics and catalytic properties of Co/TiO 2 for various rutile: anatase ratios, Catal. Commun. 6 (2005) 705–710.
[57] B. Jongsomjit, C. Sakdamnuson, P. Praserthdam, Dependence of crystalline phases in titania on catalytic properties during CO hydrogenation of Co/TiO2 catalysts, Mater. Chem. Phys. 89 (2005) 395–401.
[58] F. Diehl, A.Y. Khodakov, Promotion of cobalt Fischer-Tropsch catalysts with noble metals: a review, Oil Gas Sci. Technol.-Revue de l'IFP 64 (2009) 11–24.
[59] L.C. Almeida, O. Sanz, J. D'olhaberriague, S. Yunes, M. Montes, Microchannel reactor for Fischer–Tropsch synthesis: adaptation of a commercial unit for testing microchannel blocks, Fuel 110 (2013) 171–177.
[60] N.W. Hurst, et al., Temperature programmed reduction, Catal. Rev. Sci. Eng. 24 (2) (1982) 233–309.